



DYNAMIC PROPERTIES OF A FULL-SCALE BUILDING TESTED ON A SHAKE TABLE: FROM CONSTRUCTION TO INCIPIENT COLLAPSE

R. Astroza⁽¹⁾, F. Hernández⁽²⁾

⁽¹⁾ Assistant Professor, Faculty of Engineering and Applied Sciences, Universidad de los Andes, rastroza@miuandes.cl

⁽²⁾ Assistant Professor, Department of Civil Engineering, Universidad de Chile, fhernandezp@ing.uchile.cl

Abstract

This paper discusses the system identification of a full-scale 5-story reinforced concrete building tested on the unidirectional NHERI-UCSD shake table. The purpose of the test program, carried out in 2012, was to study the seismic response of the structure and nonstructural components and systems (NCSs) and their dynamic interaction at different levels of seismic excitation. The building specimen was tested under base-isolated (BI) and fixed-base (FB) configurations. Sequences of seismic tests of different intensities were performed for both base configurations of the building and were complemented with ambient vibration, impact/free vibration, and low amplitude white noise base excitation tests and detailed visual inspections of structural and nonstructural damage before and after each seismic test. Vibration data were collected and modal parameters of the test specimen were identified using input-output and output-only methods. Time-variant modal properties of the building during seismic tests were also identified by using an input-only methodology. The results show that the modal properties obtained by different methods are in good agreement. Moreover, the effects of nonstructural components, amplitude of excitation, nonlinear response of the isolation system, and structural/nonstructural damage progression can be related to changes in the estimated modal parameters of the building.

Keywords: System identification; Full-scale specimen; Shake table; Time-variant modal parameters; Damage



1. Introduction

System identification is an active field of research aiming to characterize the dynamic properties of large and complex civil structures by using input-output or output-only vibration data recorded by sensors installed in the structure of interest. In particular, the results obtained from system identification have been used for vibration-based damage identification purposes (e.g., [1]). The objective is to identify damage in the structure by analyzing the variation in the estimated dynamic characteristics from an initial (reference) state to a state after the structure has been subjected to potentially damage-inducing loading. The dynamic characterization of civil structures usually comprises the estimation of natural frequencies, damping ratios, and mode shapes from the recorded data. Vibration data recorded during earthquakes events on civil structures that have suffered damage is extremely scarce and large-scale shake tables have provided important data from structures tested at different states of damage and using different sources of dynamic excitation, including ambient vibrations (AV), white-noise (WN) base excitations, and seismic excitations (e.g., [2-4]). Most of previous studies have focused on the identification of the modal properties of structures using low-amplitude vibration data and a just a few researches have investigated the variations of the modal properties during strong motion earthquake excitations (e.g., [5,6]). In this paper, the modal properties of a full-scale 5-story reinforced concrete (RC) building specimen, referred to as BNCS building hereafter, tested on the large-scale UC San Diego shake table [7-9] are identified using the response data recorded during AV, WN, and seismic tests. Using the latter, the time-variant modal properties of the BNCS building are identified by using the deterministic-stochastic subspace identification method (DSI) applied to a moving short-time window of input-output acceleration data [5,6,10,11]. These modal properties are compared to those identified before and after each seismic test from AV and WN base excitation test data [12].

2. Specimen description

The test specimen was a full-scale five-story RC structure fully furnished with nonstructural components and systems (NCSs) (Fig. 1a). The height of the building was 21.34 m, distributed in five stories of 4.27 m high (Fig. 1b). The building had plan dimensions of 6.6×11.0 m in the transverse and longitudinal directions (Fig. 1c), respectively, the latter coinciding with the direction of the movement of the uni-directional shaking table.

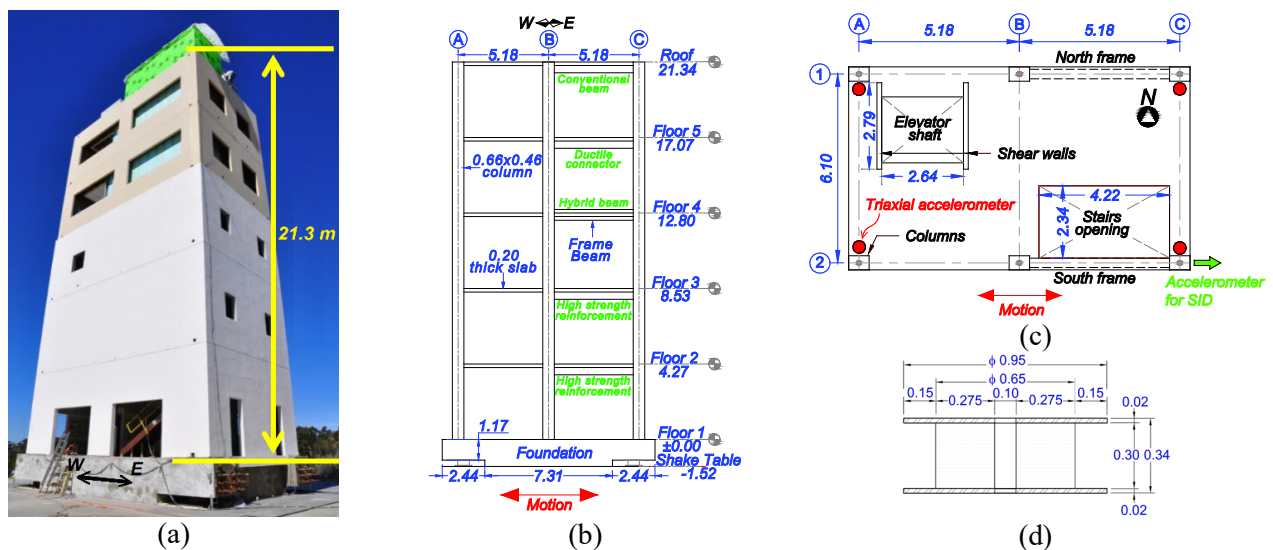


Fig. 1 – Test structure: (a) Photo of the building; (b) Plan view; (c) Elevation view; (d) schematic view of the isolator (dimensions in meters)

In the longitudinal direction, the lateral resisting system of the building consisted of a pair of one-bay special moment resisting frames. The main structural components of the building included 0.30×0.71 m beams,



0.66 × 0.46 m columns, 0.20 m thick RC floor slabs, and two 0.15 m thick RC shear walls to accommodate an operating elevator. The total weight of the building, excluding the foundation, was approximately 4420 kN, with a contribution of about 75% (3010 kN) from the bare structure and 25% (1010 kN) from the NCSs, and the weight of the foundation was 1870 kN. A pair of one-bay special moment resisting frames, one on the north face and another on the south face of the building (Fig. 1c), provided the lateral load resisting system in the longitudinal direction of the test specimen. The building was first mounted on four high-damping rubber bearings (HDRBs), which were located between the shake table platen and the foundation of the building close to the four corners of the building. The isolators had a total height of 0.34 m, comprised of 34 layers of rubber with a thickness of 6 mm each, 33 steel shim plates with a thickness of 3 mm each, and top and bottom steel plates with a thickness of 20 mm each. The isolators had a rubber diameter of 0.65 m and a core diameter of 0.10 m (Fig. 1d). More information about the specimen can be found in [7] and [8].

3. Testing protocol and instrumentation

More than 550 sensors, including displacement transducers, strain gauges, and accelerometers, were installed. In particular, four triaxial accelerometers were installed on the corners of each floor slab (see Fig. 1c) and two triaxial accelerometers were installed on the shake table platen. The seismic tests on the building were conducted in April and May, 2012. In addition to the seismic tests, AV were recorded during construction and continuously recorded from April 14 to May 18, and low-amplitude WN base excitation tests were conducted at key stages during the experimental program. Seven and six seismic input motions were applied to the base-isolated (BI) and fixed-base (FB) building, respectively. Table 1 summarizes the seismic test protocol and Fig. 2 shows the acceleration time histories (THs) and the elastic displacement response spectra (EDRS) of the seismic input motions used for the BI and FB configurations.

Table 1 – Description and nomenclature of seismic tests applied to the FB-BNCS building.

Date of test	Motion	Name	PIA (g)	PIV (mm/s)	PID (mm)
April 16, 2012	Canoga Park - 1994 Northridge EQ.	BI1-CNP100	0.21	232.7	84.2
	LA City Terrace - 1994 Northridge EQ.	BI2-LAC100	0.22	244.1	89.3
April 17, 2012	LA City Terrace - 1994 Northridge EQ.	BI3-LAC100	0.25	244.8	89.5
	San Pedro 100% - 2010 Maule (Chile) EQ.	BI4-SP100	0.52	348.7	82.7
April 26, 2012	ICA 50% - 2007 Pisco (Peru) EQ.	BI5-ICA50	0.17	223.2	47.6
April 27, 2012	ICA 100% - 2007 Pisco (Peru) EQ.	BI6-ICA100	0.32	425.9	94.6
	ICA 140% - 2007 Pisco (Peru) EQ.	BI7-ICA140	0.50	625.9	129.2
May 7, 2012	Canoga Park - 1994 Northridge EQ.	FB1-CNP100	0.21	235.0	87.8
May 9, 2012	LA City Terrace - 1994 Northridge EQ.	FB2-LAC100	0.18	230.5	93.1
	ICA 50% - 2007 Pisco (Peru) EQ.	FB3-ICA50	0.21	262.2	58.3
May 11, 2012	ICA 100% - 2007 Pisco (Peru) EQ.	FB4-ICA100	0.26	284.9	73.2
May 15, 2012	TAPS Pump Station #9 67% - 2002 Denali EQ.	FB5-DEN67	0.64	637.4	200.6
	TAPS Pump Station #9 100% - 2002 Denali EQ.	FB6-DEN100	0.80	835.7	336.2

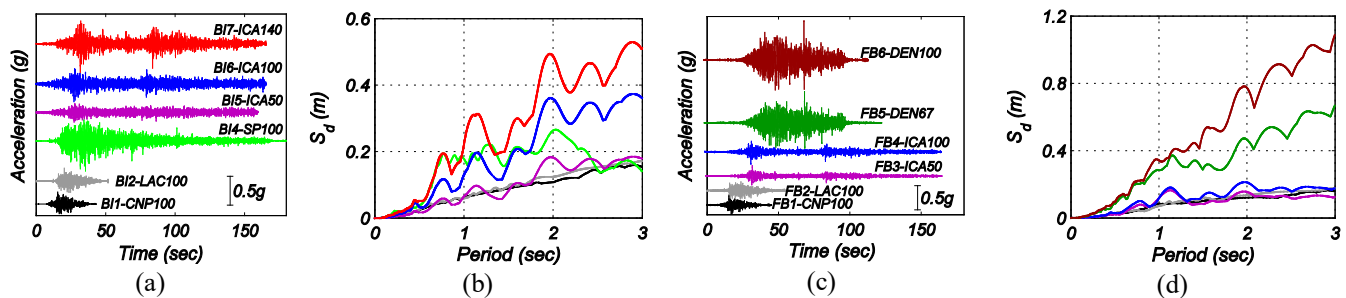


Fig. 2 – Input ground motions achieved on the shake table: (a) Acceleration TH and (b) EDRS ($\xi = 5\%$) for the BI building; (c) Acceleration TH and (d) EDRS ($\xi = 5\%$) for the FB building



3. System identification

3.1 Methods

Three output-only system identification methods were used with the recorded AV data: (i) Natural Excitation Technique combined with the Eigensystem Realization Algorithm (NExT-ERA), (ii) Stochastic Subspace Identification (SSI-DATA), and (iii) enhanced frequency domain decomposition (EFDD). The continuously recorded AV data was subdivided into contiguous (back-to-back) ten-minute long time windows referred to as data sets [13]. The identification process was performed for each of the data sets using an automated identification procedure based on stabilization diagrams [13]. In addition to these output-only methods, two input-output methods were employed with the low-amplitude white noise base excitation test data [12]: (i) Observer/Kalman Filter Identification method combined with the Eigensystem Realization Algorithm (OKID-ERA) and (ii) Deterministic-Stochastic Subspace Identification (DSI). Acceleration time histories recorded by four sensors at each level (two for each horizontal translational direction) were used to identify the modal properties of an equivalent linear time-invariant model of the building. In addition, the DSI method [14] was employed to estimate the modal properties of the building using acceleration data recorded during the seismic test (i.e., strong motion data). In this case, the variation of the modal parameters was tracked by identifying the instantaneous modal properties using input-output recorded data split on short-time windows. The acceleration at the shake table platen in the longitudinal directions was used as input data and the longitudinal acceleration responses of the south-east corner of every floor of the building were used as output data. Note that only one acceleration response per floor in the longitudinal direction of the building (direction of the input motion) was used to conduct the system identification, because (i) the differences between the longitudinal floor accelerations recorded at the four corners of each floor were negligible and (ii) measured transverse floor accelerations are very small.

3.2 Effects of nonstructural components

The instrumentation of the building began during the construction of the structure. The idea was to follow to evolution of the modal properties of the building during its construction and also to analyze in detail the effects of different nonstructural components on the dynamic characteristics of the system. To this end, AV data were recorded daily starting on August 18, 2011, before the placement of concrete of columns and walls of level 4. In addition, low amplitude WN base excitation tests were conducted for the bare structure (i.e., structure without NCSs) and for the complete building (i.e., structure incorporating all NCSs) on August 12, 2011 and February 23, 2012, respectively.

To analyze the effects of the NCSs, they were separate in sixteen main components as listed in Table 2. In Fig. 3, the evolution of the natural frequencies and damping ratios of the first three identified modes (1-T+To, 1-L, and 1-To) are shown. A very good agreement between the natural frequencies identified using SSI-DATA, NExT-ERA, and EFDD, is observed, while the identified damping ratios, ranging between 0.4 and 2.0%, exhibit a much higher method-to-method variability.

Since the partition walls modified the lateral stiffness of the building, their effect on the increase of the natural frequencies is clearly evidenced (see C1, C2, and C3 in Fig. 3). Since the mass of the building remained practically unchanged, it can be concluded that C1 to C3 increased the lateral stiffness by about 6%. Consistently, installation of interior partitions in levels 1 to 3 also increased the identified natural frequencies by increasing the initial lateral stiffness of the building by approximately 20%, while installation of the partition walls on the fourth and fifth levels (C11) also increased the natural frequencies. From December 19 to December 22, 2011, the first three modal frequencies suffered significant drops due to the placement of the precast concrete cladding panels (C9) at the fourth and fifth levels. Installation of the balloon framing (C4) between November 2 and November 23, 2011, moderately increased the first three modes natural frequencies, suggesting that its stiffening effect controlled its inertial effect due to its low weight. Ceilings (C12), penthouse (C5), and elevator cabin (C16) did not introduce modifications in the modal properties of the building because of their low masses and insignificant lateral stiffness added to the building. Regarding the damping ratios, overall, the NCSs tended to slightly increase the energy dissipation



capability of the building over time, but the effect is not clear because of the estimation uncertainty of the identified damping ratios.

Table 2 – Main NCSs installed in the BNCS building

Name	NCSs	Name	NCSs
C1	Partition walls (elevator shaft)	C9	Precast cladding (levels 4 and 5)
C2	Partition walls (stair shaft: levels 1 to 3)	C10	Elevator counterweight and rails
C3	Partition walls (stair shaft: levels 4 and 5)	C11	Interior partitions (levels 4 and 5)
C4	Balloon framing	C12	Ceilings
C5	Penthouse	C13	Sprinkler system (level 5)
C6	Interior partitions (levels 1 to 3)	C14	Roof and gas pipes (level 4)
C7	Cooling tower	C15	Contents (levels 2, 4 and 5)
C8	AHU	C16	Elevator cabin

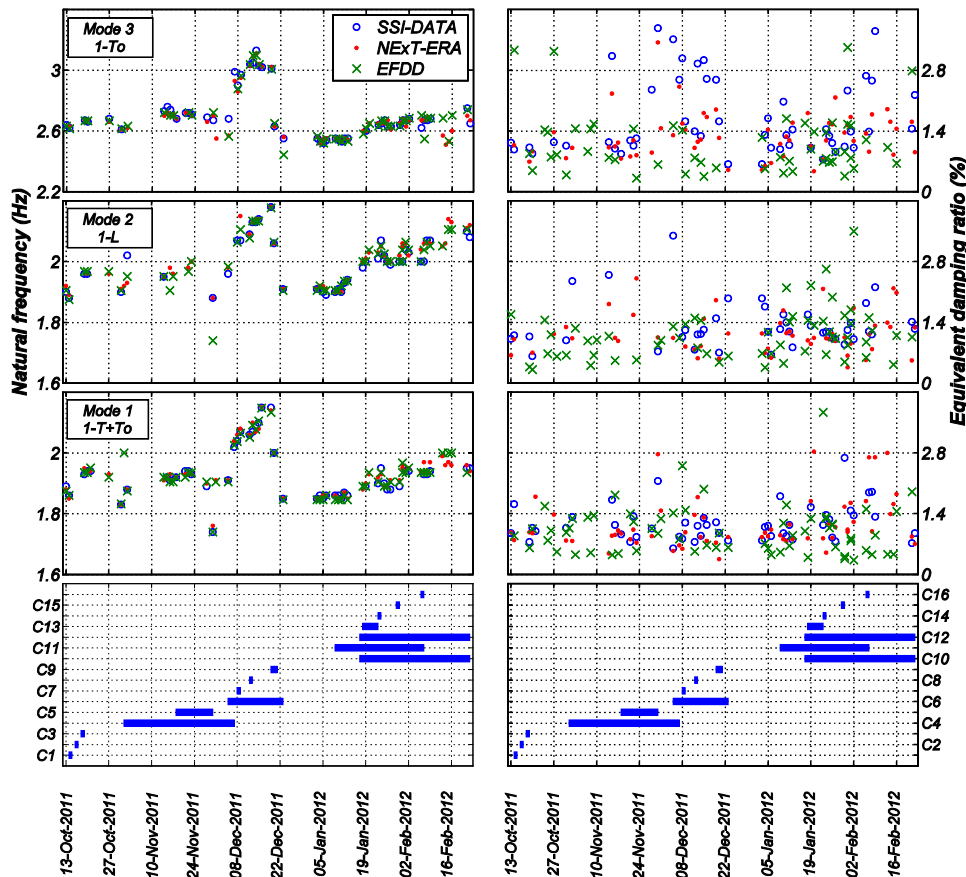


Fig. 3 – Evolution of the natural frequencies and damping ratios of the first three modes identified during installation of the main NCSs

3.3 BI building

Fig. 4 shows the first four longitudinal mode shapes (1-L, 2-L, 3-L, and 4-L) of the BI building identified using the first time window of the BII-CNP100 test. Mode 1-L involves mostly deformation of the isolation system with an almost pure rigid-body motion of the superstructure, and it is consequently referred to as isolation mode. Considerable deformation of the superstructure is observed for higher longitudinal modes (2-L, 3-L, and 4-L); however, these modes also include some deformation of the isolation system.

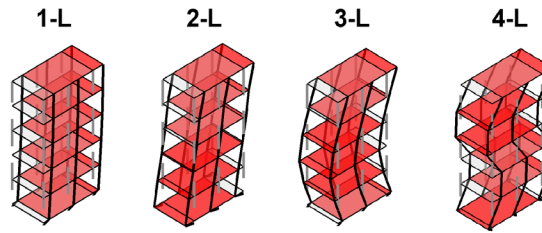


Fig. 4 – First four longitudinal modes identified for the BI building using seismic test data

In Fig. 5, the top four plots show the identified instantaneous natural frequencies of the first four longitudinal modes of the BI building, the bottom plot depicts the input acceleration time-histories achieved on the shake table and the second panel (from the bottom to the top) the effective stiffness of the isolation system. It is noted that the effective stiffness (k_{eff}) and effective damping ratio (ξ_{eff}) of an isolator under cyclic loading are calculated as [15]:

$$k_{eff} = \frac{|F^+| + |F^-|}{|\Delta^+| + |\Delta^-|} \quad ; \quad \xi_{eff} = \frac{2}{\pi} \frac{E_{loop}}{k_{eff} (|\Delta^+| + |\Delta^-|)^2}, \quad (1a,b)$$

where Δ^+ , Δ^- are the maximum (positive) and minimum (negative) horizontal displacements of the isolator during a cycle, F^+ , F^- are the maximum (positive) and minimum (negative) forces at Δ^+ , Δ^- , respectively, and E_{loop} is the energy dissipated in one hysteresis loop over displacement range from Δ^+ to Δ^- . For the seismic data, the effective properties of the isolation system (k_{eff} total) are calculated by using the total base shear (at the shake table platen) versus shear strain in the isolators hysteretic response of the building.

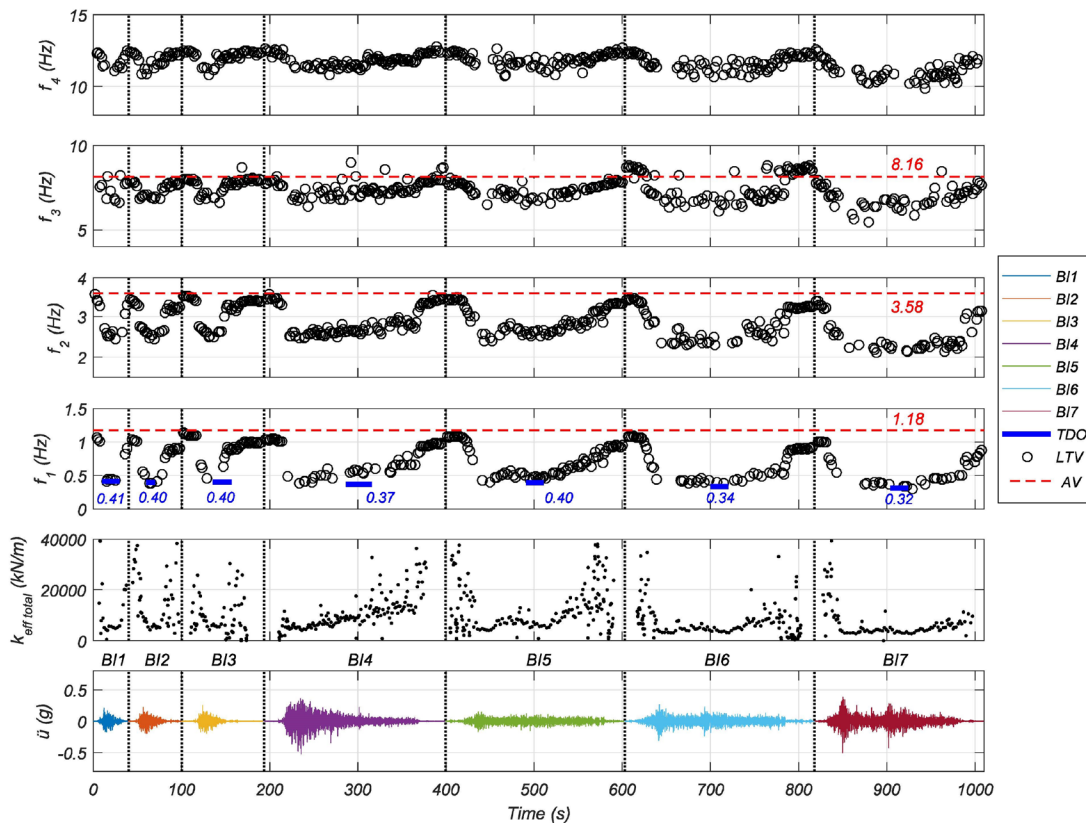


Fig. 5 – Temporal variation of the natural frequencies of the first four longitudinal modes of the BI building identified using seismic test data



In the plots of the identified natural frequencies, the frequencies identified with AV data [16] are shown with dashed red lines. The nonlinear response of the isolation system during all the seismic tests can be inferred from the variation of k_{eff} total along the time. At the beginning of each seismic test, the input motion displays low amplitudes and high values of k_{eff} total are calculated. As soon as the amplitude of the input motion increases during the strong-motion phase, the secant stiffness of the isolation system decreases significantly, but it recovers at the end of each seismic test, reaching a value similar to the one computed at the beginning of the input motion. That is, the isolation system shows a stable (i.e., without degradation) inelastic behavior. A very similar pattern is observed for the variation of the identified natural frequency of the first longitudinal mode (1-L). That is, the identified natural frequency of mode 1-L at the beginning and the end of each seismic test is similar to the frequency identified using AV data (i.e., 1.18 Hz). During the strong-motion phase, the identified natural frequency of mode 1-L decreases considerably, reaching minimum values into the range 0.37-0.41 Hz for tests BI1-CNP100 to BI5-ICA50 and 0.36 Hz and 0.32 Hz for tests BI6-ICA100 and BI7-ICA140, respectively. Because the mass of the building did not change during the tests, the frequency reduction is only explained due to the reduction of the lateral stiffness of the isolation system. That is, the lateral stiffness was reduced to values between 12% and 7% of the lateral stiffness at low-level excitations. This reduction agrees with the variation of k_{eff} total that is shown in Fig. 5.

One can note that the lower values of the identified natural frequency obtained for mode 1-L, for each ground motion, are in good agreement with the values that were reported in [17], which are shown with blue dashes lines in Fig. 5. Chen et al. [17] estimated the predominant frequency of the BI-BNCS building by using the roof displacement during the strong-motion phase obtained from collocated accelerometers and GPS antennas. The variation of the identified natural frequency of mode 1-L over time confirms that the isolation system experienced significant stiffness reduction during the seismic tests, which is almost completely recovered at the end of each seismic test. However, one can note that the identified frequency of mode 1-L at the end of a seismic test is slightly lower than that identified at the beginning of the next seismic test. This suggest that part of the stiffness degraded during a seismic test is not recovered immediately, however, it is practically completely recovered at the beginning of the next seismic test. This temporary and recoverable stiffness reduction in HDRBs is known as Mullins' effect and has been previously observed in BI structures instrumented during earthquakes (e.g., [18]).

Natural frequencies identified for higher longitudinal modes (2-L, 3-L, and 4-L) exhibit similar variations during the time, decreasing during the strong-motion part of the seismic excitations. However, for these modes the relative reduction in frequency (with respect to natural frequencies identified with low-amplitude vibration data) is much lower (relatively speaking) than the reduction observed for model 1-L. Higher modes also experience reduction in their identified natural frequencies because these modes also involve deformation of the isolation system (see Fig. 4), and not because of damage in the superstructure. An excellent agreement between the identified time-varying natural frequencies at the beginning and end of seismic tests and those identified from AV [16] is also observed for higher modes. The identification of almost the same natural frequencies for all longitudinal modes at the beginning of the first seismic test (BI1-CNP100) and at the end of the last seismic test (BI7-ICA140) suggests that the building did not suffer reduction of stiffness during the strong motions, which means that the building did not suffer structural damage. This conclusion is in agreement with the low demands of the building, at the global and local levels, reported in Astroza et al. [6], and also with the visual inspections conducted after seismic test BI7-ICA140. The top four plots of Fig. 6 show the instantaneous identified equivalent viscous damping ratios for the first four longitudinal modes of the BI building. In these plots, the damping ratios identified with AV data by Astroza et al. [16] are displayed with dashed red lines. Similarly, the damping ratio of the predominant mode estimated during the strong-motion phase by using the roof displacement that was obtained by Chen et al. [17] is depicted with blue dashed lines. The bottom and second (from bottom to top) plots show the input motion time-histories that were achieved on the shake table and the effective damping (ξ_{eff}) computed by using the hysteretic response of the isolation layer according to the procedure that was previously explained.

The damping ratio identified for mode 1-L is significantly larger than those identified for higher modes, and its values during the strong-motion phase correlates properly with ξ_{eff} . For mode 1-L, the identified damping



ratio increases considerably from values around 5% during the beginning of the input motions to values as large as 12-25% during the strong-motion phase, and then these values decrease again during the end of the seismic tests, reaching values around 5%. This damping ratio is in excellent agreement with the damping ratio of mode 1-L that was identified with AV data ($\xi=5.3\%$). Mode 1-L comprises large shear deformation of the bearings (Fig. 4) and is highly related to the hysteretic response of the isolation system. Because of the underlying mathematical model considered in the system identification method employed here, all the sources of energy dissipation, in particular the energy dissipated by the bearings, are identified as an equivalent viscous damping. It is noted that the damping ratios identified for mode 1-L during the strong motion phase of the seismic excitations are slightly larger than those computed from the hysteretic response of the isolation system. Damping ratios identified for higher longitudinal modes (2-L, 3-L, and 4-L) are considerably lower than those identified for mode 1-L. For mode 2-L, the identified damping ratio varies from 2.5% to 8.5% and for modes 3-L and 4-L between 1.0 and 5.0%. Although damping ratios of higher modes also tend to increase during the strong-motion phase of the imposed input motion, they do not vary at the same scale as that of mode 1-L.

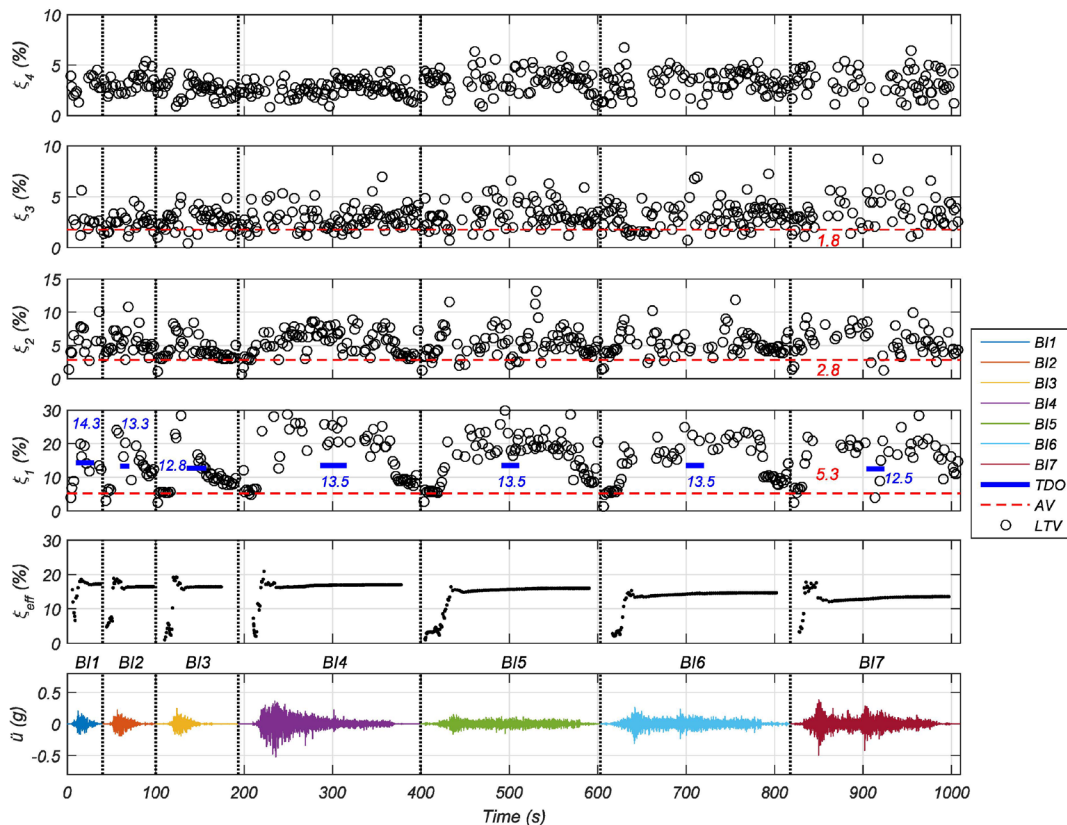


Fig. 6 – Temporal variation of the damping ratios of the first four longitudinal modes of the BI building identified using seismic test data

3.3 FB building

Based on system identification analyses conducted for the fixed-base BNCS building using AV and WN base excitation test data [12], modes with natural frequencies below 15 Hz were analyzed. It is noted that the frequency range from 0 to 15 Hz includes the first three longitudinal modes of the building (1-L, 2-L, and 3-L). Only longitudinal modes are identified with the seismic data because the shaking direction was imposed in that direction, therefore, the identification associated with transverse and torsional modes is not plausible because of their low contribution to the dynamic response of the building. The mode shapes identified for the first time window of the FB1-CNP100 test are shown in Fig. 7.

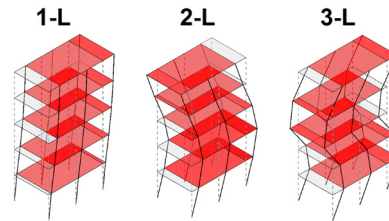


Fig. 7 – First four longitudinal modes identified for the FB building using seismic test data

The bottom panel of Fig. 8 depicts the input acceleration time-histories measured on top of the foundation (floor 1) and upper panels show the natural frequencies of the first three longitudinal modes of the building identified using the short-time window approach described above. In these plots, natural frequencies of the corresponding modes identified with AV and WN base excitation data reported in [12] are marked with green and red dashes, respectively, at the beginning and at the end of each seismic test. In addition, for the fundamental mode (1-L), black dashes during the strong motion phases report the identification results obtained in Chen et al. [17] by using an optimization approach based on the roof displacement measured from collocated accelerometers and GPS antennas.

It is noted that at the beginning of each seismic test, the input motion exhibits low amplitudes and the identified natural frequencies match very well those identified using AV data (green dashes) and are higher than those identified using WN base excitation data (red dashes). As the amplitude of the base excitation increases, the identified natural frequencies decrease significantly, but they recover toward the end of each test, reaching a value lower than that identified at the beginning of the same seismic test but significantly higher than the lowest frequencies values identified for the corresponding test. This implies that the equivalent lateral stiffness of the building decreases significantly during the strong motion phase (because of nonstructural and structural damage) but then it increases when the amplitude of the excitation decreases at the end of the seismic test. This behavior suggests that cracks in the concrete are opened during the strong motion phase and then they close after the amplitude of the excitation becomes small. However, some permanent degradation of the stiffness is observed, because the frequencies identified at the end of each seismic test are lower than those identified at the beginning of the same test. The same pattern is observed for the three longitudinal models. For model 1-L, at the beginning of test FB1-CNP100 a natural frequency 1.67 Hz is identified, progressively decreasing at the end of each of the seismic tests, and reaching a value of 0.73 Hz at the end of the final test FB6-DEN1100. Similarly, modes 2-L and 3-L progress from 6.77 and 10.88 Hz at the beginning of test FB1-CNP100 to 3.7 and 6.78 Hz at the end of test FB6-DEN100, respectively. For the first four tests (FB1-CNP100 to FB4-ICA100), the natural frequency of mode 1-L identified in this work in the strong motion phase and that obtained by Chen et al. [17] are in very good agreement.

Fig. 9 shows the identification results for the equivalent viscous damping ratios. In the top three plots, the identified damping ratios for modes 1-L, 2-L, and 3-L are shown. Consistently with Fig. 8, identification results from AV and WN test data [16] and those reported in [17] for the strong motion parts of the first four tests are included in the plots with dashed lines. Significant variations of the identified damping ratios are observed. In general, they tend to increase during the strong motion phase for all modes. In addition, the values identified at the beginning and end of the seismic tests are relatively close to those identified when AV data was employed. It is noted that identification results obtained using AV data are affected by environmental conditions, and, in particular, the effects on damping ratios are significant [13]. As the seismic demand induced by the seismic excitation increases (from FB1-CNP100 to FB6-DEN100), the identified damping ratios also increase, suggesting that a larger amount of energy is dissipated when the excitation increases. It is worthy to note that the underlying mathematical model considered in the system identification method used, assumed that all the sources of energy dissipation are identified as equivalent viscous damping. For mode 1-L, the average value of the identified damping ratio in the strong motion part of the excitations is about 5-7% for the first four tests (FB1-CNP100 to FB4-ICA100) and increases to about 8 and 10% for tests



FB5-DEN67 and FB6-DEN100, respectively. Similar values and trend are observed for the damping ratios identified for mode 2-L, while the damping ratio variation associated with mode 3-L is smaller.

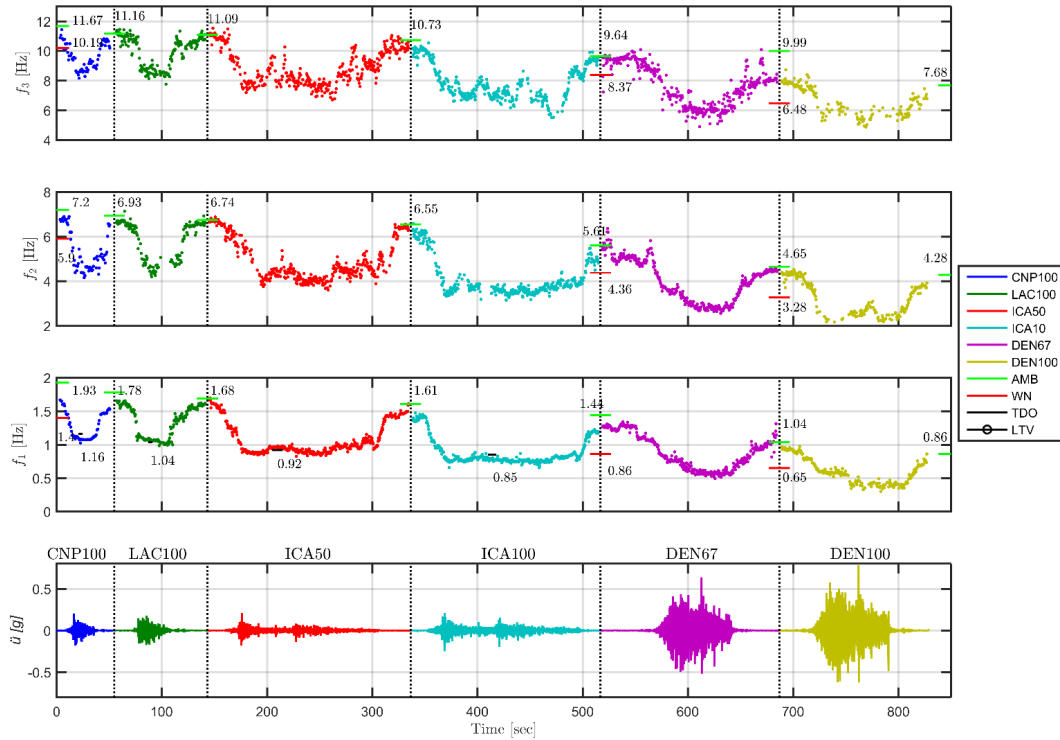


Fig. 8 – Temporal variation of the natural frequencies of the first three longitudinal modes of the FB building identified using seismic test data

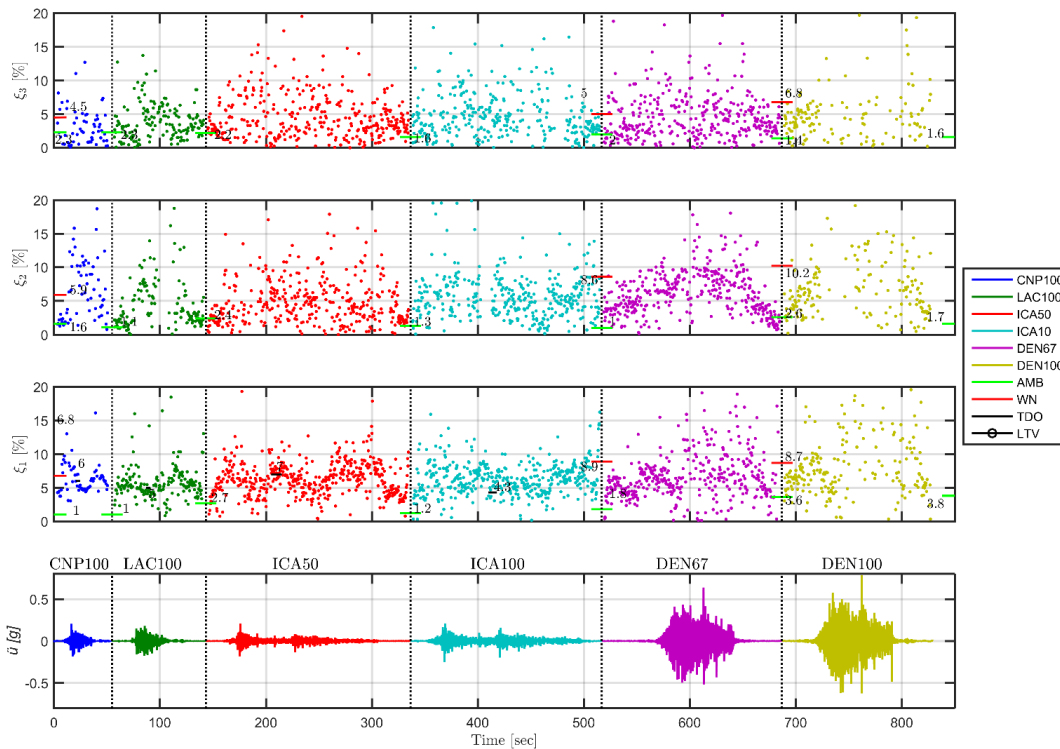


Fig. 9 – Temporal variation of the damping ratios of the first four longitudinal modes of the FB building identified using seismic test data



4. Acknowledgements

The authors are very grateful to Professors Tara C. Hutchinson, Joel P. Conte, and José I. Restrepo from the University of California, San Diego for making these data available. R. Astroza acknowledges the financial support from the Chilean National Commission for Scientific and Technological Research (CONICYT), FONDECYT project No. 11160009.

5. References

- [1] Fan W, Qiao PZ (2011): Vibration-based damage identification methods: a review and comparative study. *Structural Health Monitoring*, **10** (5), 83–111.
- [2] Ji X, Fenves G, Kajiwara K, Nakashima, M (2011): Seismic damage detection of a full-scale shaking table test structure.” *ASCE Journal of Structural Engineering*, **137** (1), 14–21.
- [3] Moaveni B, He X, Conte JP, Restrepo JI, Panagiotou M (2011): System identification study of a seven-story full-scale building slice tested on the UCSD-NEES shake table. *ASCE Journal of Structural Engineering*, **137** (6), 705–717.
- [4] Astroza R., Ebrahimian H, Conte JP, Restrepo JI, Hutchinson, TC (2016): Influence of the construction process and nonstructural components on the modal properties of a five-story building. *Earthquake Engineering & Structural Dynamics*, **45** (7), 1063–1084.
- [5] Loh C-H, Weng J-H, Chen C-H, Lu K-C (2013): System identification of mid-story isolation building using both ambient and earthquake response data. *Structural Control and Health Monitoring*, **20** (2), 139–155.
- [6] Astroza R, Gutierrez G, Repenning C, Hernández F (2018): Time-variant modal parameters and response behavior of a base-isolated building tested on a shake table. *Earthquake Spectra*, **34** (1), 121–143.
- [7] Chen MC, Pantoli E, Wang X, Astroza R, Ebrahimian H, Hutchinson TC, Conte JP, Restrepo JI, Marin C, Walsh K, Bachman R, Hoehler M, Englekirk R, Faghihi M (2016): “Full-scale structural and nonstructural building system performance during earthquakes: Part I – Specimen description, test protocol, and structural response.” *Earthquake Spectra*, **32** (2), 737–770.
- [8] Pantoli E, Chen MC, Wang X, Astroza R, Ebrahimian H, Hutchinson TC, Conte, JP, Restrepo JI, Marin C, Walsh K, Bachman R, Hoehler M, Englekirk R, Faghihi M (2016): “Full-scale structural and nonstructural building system performance during earthquakes: Part II – NCS damage states.” *Earthquake Spectra*, **32** (2), 771–794.
- [9] Pantoli E, Chen MC, Hutchinson TC, Astroza R, Conte JP, Ebrahimian H, Restrepo JI, Wang X (2016): Landmark dataset from the building nonstructural components and systems (BNCS) project. *Earthquake Spectra*, **32** (2), 1239–1260.
- [10] Tobita J, Izumi M, Katukura H. (1988): Identification of vibration systems and nonlinear dynamics characteristics of structures under earthquake excitations. *9th World Conference on Earthquake Engineering*, Tokyo-Kyoto, Japan.
- [11] Moaveni B, Asgari E (2012): Deterministic-stochastic subspace identification method for identification of nonlinear structures as time-varying linear systems. *Mechanical Systems and Signal Processing*, **31**, 40–55.
- [12] Astroza R, Ebrahimian H, Conte JP, Restrepo JI, Hutchinson TC (2016): System identification of a full-scale five-story reinforced concrete building tested on the NEES-UCSD shake table. *Structural Control and Health Monitoring*, **23** (3), 535–559.
- [13] Astroza R, Ebrahimian H, Conte JP, Restrepo JI, Hutchinson TC (2013): Statistical analysis of the identified modal properties of a 5-story RC seismically damaged building specimen. *11th International Conference on Structural Safety and Reliability (ICOSSAR'13)*, New York, NY.
- [14] Van Overschee P, De Moor B (1996): *Subspace Identification for Linear Systems: Theory, Implementation, Applications*. Kluwer Academic Publishers, The Netherlands.
- [15] American Society of Civil Engineers (ASCE) (2010): *Minimum Design Loads for Buildings and Other Structures*. ASCE/SEI 7-10, Reston, VA.



- [16] Astroza R, Ebrahimian H, Conte JP, Restrepo JI, Hutchinson TC (2020): Seismic response analysis and modal identification of a full-scale five-story base-isolated building tested on a shake table. Submitted to *Journal of Sound and Vibration*.
- [17] Chen MC, Astroza R, Restrepo JI, Conte JP, Hutchinson TC, Bock Y (2017): Predominant period and equivalent viscous damping ratio identification on a full-scale building shake table test. *Earthquake Engineering & Structural Dynamics*, **46** (14), 2459–2477.
- [18] Siringoringo D, Fujino Y (2014): Long-term seismic monitoring of base-isolated building with emphasis on serviceability assessment. *Earthquake Engineering & Structural Dynamics*, **44** (4), 637–655.